RSC Advances

PAPER

View Article Online
View Journal | View Issue

Cite this: *RSC Adv.*, 2025, **15**, 42900

Aromatic C–H hydroxylation reactions catalysed by nickel(II) complexes of monoanionic ligands

Anjana Rajeev, [a] Sethuraman Muthuramalingam [b] and Muniyandi Sankaralingam *[a]

Received 23rd September 2025
Accepted 27th October 2025

DOI: 10.1039/d5ra07204b

rsc.li/rsc-advances

The selective conversion of benzene to phenol in a single step under mild reaction conditions could serve as a viable alternative to the cumene process. Herein, we report the catalytic activity of nickel(II) complexes of the type $[Ni(L)(H_2O)]ClO_4$ (**1–3**) containing monoamidate pentadentate N5 ligands (L1(H)–L3(H)) in the oxidation of aromatic C–H bonds using H_2O_2 as the oxidant. Catalytic conditions were optimised by studying the effect of catalyst loading, H_2O_2 amount, temperature and reaction time. Among the series, catalyst **1** showed the best activity under optimised reaction conditions with a phenol yield of 24.6%, selectivity of 98%, and a turnover number (TON) of 492. Ligand donor moiety influence on the catalytic performances was evident as the substitution of one pyridyl moiety in catalyst **1** with imidazolyl methyl (**2**) or 6-methyl pyridyl 1-methyl (**3**) groups resulted in diminished catalytic performance. Furthermore, kinetic isotopic effect (KIE = 1.04) and radical trapping studies ruled out discarded the involvement of hydroxyl or carbon-centred radicals in the oxidation reaction. Moreover, preferential phenol formation over side-chain oxidation, as well as the product distribution pattern obtained during the oxidation of other aromatic substrates, suggested the electrophilic aromatic substitution pathway mediated by a nickel-oxygen species.

1 Introduction

Phenol is a chemical of key relevance owing to its ubiquitous usage in synthesising resins, plastics, agrochemicals, dyes, and pharmaceuticals.[1] Currently, the worldwide production of phenol is predominantly from the three-step cumene process reported by Hock and Lang.[2] However, in addition to its multi-step nature, the cumene process has some other disadvantages, such as the requirement of harsh reaction conditions and the equimolar production of acetone.[1,3] On the other hand, enzymes such as cytochrome P450 mediate the aromatic functionalisation reactions under physiological conditions by utilising molecular oxygen.[4–7] In this context, developing bioinspired model compounds of such enzymes for the single-step conversion of benzene to phenol has elicited considerable research interest.[3] Intriguingly, numerous first–row transition metal complexes have long been known to mimic the functions of several natural enzymes and have shown promising activity in a variety of organic transformations.[7–19] The catalytic potential of different manganese, iron, cobalt, nickel, and copper complexes has been explored in the oxidation of arenes under mild reaction conditions using molecular oxygen or hydrogen peroxide.[3,20–22]

Although only a limited number of nickel catalysts have been reported for aromatic oxidation reactions, the steric and electronic properties of ligands have been found to impact the catalytic performances of the complexes.[23–25] However, most of the employed ligands were tetradentate with pyridyl or alkylamine donors.[23–25] Also, an ambiguity in the active oxidant responsible for the hydroxylation is evident in these studies, as different intermediates such as dinickel(III)bis(μ-oxo) complex, nickel nanoparticles and nickel-oxyl compound were proposed as the reactive species.[23–26] Interestingly, nickel complexes bearing pentadentate ligands are known to show promising activity in alkane hydroxylation and olefin epoxidation reactions.[27–30] Very recently, we reported that the neutral pentadentate nickel complexes can show excellent activity in both alkane and aromatic oxidation *via* the nickel(II)-oxyl intermediate.[27,28]

The monoanionic pentadentate nickel(II) complex reported by Kim *et al.* has displayed good activity in olefin epoxidation.[29] Moreover, manganese complexes supported by such ligand systems are found to display excellent activity in electrophilic, nucleophilic, and redox reactions.[31–33] The selective alkane hydroxylation reactivity of iron monoamidate pentadentate complexes is also known in the literature.[33,35] However, complexes with such ligand architectures have not yet been explored for benzene oxidation reactions with any metal.

[a]*Bioinspired & Biomimetic Inorganic Chemistry Laboratory, Department of Chemistry, National Institute of Technology Calicut, Kozhikode, Kerala 673601, India. E-mail: msankaralingam@nitc.ac.in; sankarjan06@gmail.com*

[b]*Institut de Química Computacional i Catalisi; (IQCC), Departament de Química, Universitat de Girona, Girona E-17003, Catalonia, Spain*

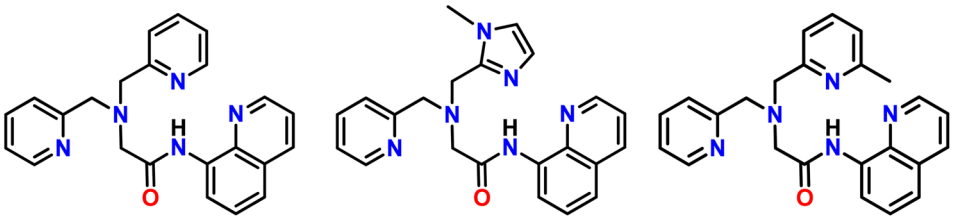

Scheme 1 The structure of the ligands L1(H)–L3(H) is discussed in this study.

With our ongoing interest in this field and in developing amidate ligand architectures, we systematically designed, synthesised, and characterised a series of nickel(II) complexes (**1–3**) bearing monoamidate pentadentate ligands (L1(H)–L3(H), Scheme 1) and probed their catalytic activity in one-step benzene hydroxylation using H_2O_2 as the oxidant. The reaction conditions, such as catalyst loading, oxidant concentration, reaction time, and temperature, were optimised using catalyst **1**. Complexes showed catalytic activity in the order **1** > **2** > **3** with a remarkable phenol selectivity of 98%. The best catalyst **1** was further used for the oxidation of substituted benzenes and afforded corresponding phenols with appreciable selectivity. Also, kinetic isotopic effect measurement in the presence of catalyst **1** revealed the inverse kinetic isotopic effect, suggesting an electrophilic aromatic substitution pathway for the hydroxylation reaction. Based on the experimental results, a plausible mechanism is proposed in which a nickel-oxyl species mediates the oxidation reaction.

2 Experimental

2.1 Materials

All chemicals were purchased from commercial sources as reagent grade and used directly without further purification unless otherwise specified. Nickel(II) perchlorate hexahydrate, pyridine-2-carboxaldehyde, and sodium borohydride were purchased from Alfa Aesar. 1-methylimidazole-2-carboxaldehyde, 6-methyl-2-pyridinecarboxaldehyde, 2-aminomethyl pyridine, 8-aminoquinoline, 2-bromoacetylbromide were purchased from TCI. Sodium carbonate, sodium sulfate, benzene, toluene, ethylbenzene, cumene, anisole, nitrobenzene, chlorobenzene, hydrogen peroxide, and triethylamine were purchased from Merck and used as such. Dichloromethane, ethyl acetate, and hexane were purchased from Qualigens and used as such. Methanol was purchased from Qualigens and distilled over iodine (1 equiv.) and magnesium turnings (10 equiv.) before use. Acetonitrile was purchased from Emplura and distilled over calcium hydride before use.

Caution note! Perchlorate salts are explosive; suitable precautions should be taken when handling them.

2.2 Physical measurements

The electronic spectra of the complexes were recorded using an Agilent Cary 8454 UV-Visible diode array spectrophotometer, using distilled acetonitrile as the solvent at 298 K. The ATR spectra of the ligands and complexes were recorded using an Agilent Cary-630 FTIR instrument in the 4000 to 400 cm^{-1} range. The ^{1}H- and ^{13}C- NMR spectra of ligands L1(H)–L3(H) were recorded using a Jeol 500 MHz instrument, with deuterated dimethyl sulfoxide as the solvent, and tetramethylsilane as the internal standard. The CHN analysis was done using a PerkinElmer 2400 Series II CHN analyser. The mass data of the complexes were recorded using the Waters Synapt XS HRMS instrument. Product analysis of aromatic oxidation reactions was conducted using Agilent 5977E GC/MSD with an HP-5 MS ultra-inert (30 m × 250 μm × 0.25 μm) capillary column and Agilent 8860 GC series equipped with an FID detector and an HP-5 GC column (30 m × 0.32 mm × 0.25 μm).

2.3 Synthesis of ligands

The ligands L1(H), L2(H), and L3(H) (Scheme 1) were synthesised by the following reports.[31–36] All the ligands were synthesised in three steps. The first step involves the synthesis of 2-bromo-*N*-(quinoline-8-yl)acetamide, and the second step consists of the synthesis of bis(pyridine-2-ylmethyl)amine. Finally, in the third step, the compounds obtained from steps 1 and 2 undergo dehydrohalogenation to form L1(H). Similarly, ligands L2(H) and L3(H) (Scheme 1) were synthesised by modifying the procedure used for the synthesis of L1(H).

2.3.1 Synthesis of 2-(bis(pyridin-2-ylmethyl)amino)-*N*-(quinolin-8-yl)acetamide (L1(H))

2.3.1.1 Synthesis of 2-bromo-N-(quinoline-8-yl)acetamide (BrQ). Synthesis was done by adapting the method available in the literature as follows.[34] Bromoacetyl bromide (1.6 g, 8.3 mmol) was slowly added to an acetonitrile solution of 8-aminoquinoline (1.0 g, 6.9 mmol) and sodium carbonate (1.2 g, 11.2 mmol) in ice-cold conditions under a nitrogen atmosphere. The resultant mixture was stirred for 20 minutes, and sodium carbonate in the final reaction mixture was removed by Celite filtration. The filtrate was then rotary evaporated to get BrQ as a yellow crystalline powder. Yield: 1.5 g, 82(2)%.

2.3.1.2 Synthesis of bis(pyridine-2-ylmethyl)amine. The compound was synthesised according to the literature methods.[36] 2-aminomethyl pyridine (0.540 g, 5 mmol) was added to a methanolic solution of pyridine-2-carboxaldehyde (0.535 g, 5 mmol) and stirred overnight. After that, $NaBH_4$ (0.226 g, 6 mmol) was added to the reaction mixture in ice-cold conditions, and the stirring was continued for another 12 h at

room temperature. The resulting reaction mixture was rotary evaporated to dryness, and the crude product was dissolved in water and then extracted with dichloromethane (50 mL × 3). The collected organic fraction was dried over anhydrous sodium sulfate and rotary evaporated to get a yellow oil. Yield 0.95 g, 95(3)%.

2.3.1.3 Synthesis of 2-(bis(pyridin-2-ylmethyl)amino)-N-(quinolin-8-yl)acetamide (L1(H)). Bis(pyridin-2-ylmethyl)amine (0.54 g, 2.7 mmol) was added to an acetonitrile solution containing BrQ (0.45 g, 1.6 mmol) and sodium carbonate (0.22 g, 2 mmol) in an ice bath under a nitrogen atmosphere. The reaction mixture was stirred for 12 h by maintaining the inert atmosphere and ice-cold conditions. The crude product obtained after rotary evaporation was purified using column chromatography (alumina, hexane/ethylacetate (v/v = 1 : 1)).[34] Yield 0.53 g, 86(3)%. ATR-IR, cm^{-1} (Fig. S1(top)): 3315 ν(NH), 1671 ν(C=O). ^{1}H NMR (500 MHz, DMSO-d_6) (Fig. S2): (δ_H ppm) 11.44 (s, 1H), 9.02 (dd, 1H), 8.57 (dd, 1H), 8.43 (d, 2H), 8.38 (d, 1H), 7.84 (d, 2H), 7.75 (td, 2H), 7.65–7.61 (m, 2H), 7.52 (t, 1H), 7.22–7.19 (m, 2H), 3.91 (s, 4H), 3.49 (s, 2H). ^{13}C NMR (125 MHz, DMSO-d_6) (Fig. S3): (δ_C ppm) 169.0, 157.9, 149.5, 149.4, 138.4, 137.2, 137.1, 134.5, 128.3, 127.6, 123.7, 123.0, 122.8, 122.3, 115.9, 60.2, 58.8.

2.3.2 Synthesis of 2-(((1-methyl-1*H*-imidazol-2-yl)methyl)(-pyridin-2-ylmethyl)amino)-*N*-(quinolin-8-yl)acetamide (L2(H))

2.3.2.1 Synthesis 1-(1-methyl-1H-imidazole-2-yl)-N-(pyridine 2ylmethyl)methanamine. The compound was synthesised according to the literature procedure.[36] 2-aminomethyl pyridine (0.490 g, 4.54 mmol) was added to a methanolic solution of 1-methyimidazole-2-carboxaldehyde (0.50 g, 4.54 mmol), and the reaction mixture was stirred overnight. After that, $NaBH_4$ (0.206 g, 5.45 mmol) was added to the reaction mixture in ice-cold conditions, and stirring was continued for another 12 hours. The final reaction mixture was rotary evaporated to dryness and extracted with dichloromethane (50 mL × 3). The collected organic fraction was dried over anhydrous sodium sulfate and rotary evaporated to get a yellow oil. Yield 0.58 g, 63(2)%.

2.3.2.2 Synthesis of 2-(((1-methyl-1H-imidazol-2-yl)methyl)(-pyridin-2-ylmethyl)amino)-N-(quinolin-8-yl)acetamide (L2(H)). L2(H) was synthesised by adapting the same procedure used to prepare L1(H).[34] 1-(1-methyl-1*H*-imidazol-2-yl)-*N*-(pyridin-2-ylmethyl)methanamine (0.62 g, 3 mmol) was added to an acetonitrile solution containing BrQ (0.54 g, 2.7 mmol) and sodium carbonate (0.24 g, 2.29 mmol) in an ice bath under a nitrogen atmosphere. The reaction mixture was stirred for 12 h by maintaining the inert atmosphere and the ice-cold condition. The crude product obtained after rotary evaporation was purified using column chromatography (alumina, ethylacetate/methanol (v/v = 49 : 1)). Yield 0.66 g, 63(2) %. ATR-IR, cm^{-1} (Fig. S4(top)): 3303 ν(NH), 1681 ν(C=O). ^{1}H NMR (500 MHz, DMSO-d_6) (Fig. S5): (δ_H ppm) 11.06 (s, 1H), 8.93 (dd, 1H), 8.54 (dd, 1H), 8.44 (d, 1H), 8.37 (dd, 1H), 7.81 (d, 1H), 7.72 (td, 1H), 7.64–7.60 (m, 2H), 7.51 (t, 1H), 7.22–7.20 (m, 1H), 6.94 (s, 1H), 6.69 (s, 1H), 3.91 (s, 2H), 3.81 (s, 2H), 3.62 (s, 3H), 3.47 (s, 2H). ^{13}C NMR (125 MHz, DMSO-d_6) (Fig. S6): (δ_C ppm) 169.5, 158.2, 149.3, 149.3, 144.5, 138.2, 137.2, 137.1, 134.5, 128.3, 127.6, 127.0, 124.2, 123.1, 122.8, 122.2, 115.9, 61.1, 58.2, 49.9, 32.4.

2.3.3 Synthesis of 2-(((6-methylpyridin-2-yl)methyl)(-pyridin-2-ylmethyl)amino)-*N*-(quinolin-8-yl)acetamide (L3(H))

2.3.3.1 Synthesis of 1-(6-methylpyridin-2-yl)-N-(pyridin-2-ylmethyl)methanamine. 2-aminomethyl pyridine (0.27 g, 2.5 mmol) was added to a methanolic solution of 6-methyl-2-pyridinecarboxaldehyde (0.30 g, 2.5 mmol), and the reaction mixture was stirred overnight. After that, $NaBH_4$ (0.113 g, 3 mmol) was added to the reaction mixture under ice-cold conditions, and stirring was continued for another 12 hours. The final reaction mixture was rotary evaporated to dryness and extracted with ethyl acetate (50 mL × 3). The collected organic fraction was dried over anhydrous sodium sulfate and rotary evaporated to get a yellow oil. Yield 0.48 g, 90(2)%. ^{1}H NMR (500 MHz, $CDCl_3$) (Fig. S7): (δ_H ppm) 8.46 (d, 1H), 7.56 (td, 1H), 7.44 (t, 1H), 7.27 (d, 1H), 7.09–7.06 (m, 2H), 6.92 (d, 1H), 3.90 (s, 2H), 3.86 (s, 2H), 3.32 (s, 1H), 2.45 (s, 3H). ^{13}C NMR (125 MHz, DMSO-d_6) (Fig. S8): (δ_C ppm) 159.5, 158.7, 158.0, 149.2, 136.8, 136.6, 122.4, 122.0, 121.6, 119.3, 54.7, 54.7, 24.4.

2.3.3.2 Synthesis of 2-(((6-methylpyridin-2-yl)methyl)(pyridin-2-ylmethyl)amino)-N-(quinolin-8-yl)acetamide (L3(H)). L3(H) was synthesised by adapting the same procedure used to prepare L1(H).[34] 1-(6-methylpyridin-2-yl)-*N*-(pyridin-2-ylmethyl) methanamine (0.29 g, 1.35 mmol) was added to an acetonitrile solution containing BrQ (0.30 g, 1.13 mmol) and sodium carbonate (0.144 g, 1.36 mmol) in an ice bath under nitrogen atmosphere. The reaction mixture was stirred for 12 h by maintaining the inert atmosphere and ice-cold conditions. The crude product obtained after rotary evaporation was purified using column chromatography (alumina, hexane/ethyl acetate (v/v = 1 : 1)). Yield 0.28 g, 62(2) %. ATR-IR, cm^{-1} (Fig. S9(top)): 3298 ν(NH), 1681 ν(C=O). ^{1}H NMR (500 MHz, DMSO-d_6) (Fig. S10): (δ_H ppm) 11.43 (s, 1H), 9.01 (dd, 1H), 8.56 (dd, 1H), 8.43 (d, 1H), 8.37 (dd, 1H), 7.89 (d, 1H), 7.74 (td, 1H), 7.65–7.61 (m, 4H), 7.50 (t, 1H), 7.21–7.18 (m, 1H), 7.04–7.00 (m, 1H), 3.91 (s, 2H), 3.85 (s, 2H), 3.46 (s, 2H), 2.29 (s, 3H). ^{13}C NMR (125 MHz, DMSO-d_6) (Fig. S11): (δ_C ppm) 169.6, 158.5, 157.7, 149.5, 149.4, 138.4, 137.4, 137.2, 137.1, 134.5, 128.3, 127.5, 123.7, 123.0, 122.8, 122.3, 122.1, 120.5, 115.9, 60.9, 60.9, 59.4, 23.9.

2.4 Isolation of the nickel(II) complexes

The present complexes **1–3** were isolated according to the literature methods for synthesising nickel complexes.[27,36–41] A methanolic solution (1 mL) of the ligand (L1(H)–L3(H)) (0.5 mmol) was added to $Ni(ClO_4)_2 \cdot 6H_2O$ (0.5 mmol) dissolved in 1 mL of methanol. Triethylamine (TEA, 0.5 mmol) was added to this reaction mixture. After 1 hour, the pink precipitate formed was filtered through a sintered crucible and washed with a cold methanol-diethyl ether mixture. The pink precipitate was dried under a vacuum.

2.4.1 [Ni(L1)(H_2O)](ClO_4) (1). Complex **1** was prepared using the above general procedure using L1(H). Yield 79(2)%. ATR-IR, cm^{-1}(Fig. S1 (bottom)): 3435 ν(OH), 1602 ν(CO), 1095, 976, 621 ν(ClO_4^-). HR-MS (Fig. S12): m/z = 440.1020 $[Ni(L1)]^+$ (calcd = 440.1021), m/z = 220.5544 $[Ni(L1(H))]^{2+}$ (calcd =

220.5550). Elemental analysis calcd for $C_{23}H_{22}ClN_5NiO_6$: C, 49.45; H, 3.97; N, 12.54, found: C, 49.48; H, 3.93; N, 12.50.

2.4.2 [Ni(L2)(H$_2$O)](ClO$_4$) (2). Complex **2** was prepared using the above general procedure using L2(H). Yield 72(2)%. ATR-IR, cm^{-1} (Fig. S4 (bottom)): 3484 ν(OH), 1600 ν(CO), 1091, 976, 626 ν(ClO_4^-). HR-MS (Fig. S13): m/z = 443.1124 $[Ni(L2)]^+$ (calcd = 443.1130, m/z = 222.0604 $[Ni(L2(H))]^{2+}$ (calcd = 222.0605). Elemental analysis calcd for $C_{22}H_{23}ClN_6NiO_6$: C, 47.05; H, 4.13; N, 14.96, found: C, 47.08; H, 4.16; N, 14.91.

2.4.3 [Ni(L3)(H$_2$O)](ClO$_4$) (3). Complex **3** was prepared using the above general procedure using L3(H). Yield 74(2)%. ATR-IR, cm^{-1} (Fig. S9(bottom)): 3431 ν(OH), 1604 ν(CO), 1100, 976, 626 ν(ClO_4^-). HR-MS (Fig. S14): m/z = 454.1192 $[Ni(L3)]^+$ (calcd = 454.1178), m/z = 227.5633 $[Ni(L3(H))]^{2+}$ (calcd = 227.5628). Elemental analysis calcd for $C_{24}H_{24}ClN_5NiO_6$: C, 50.34; H, 4.22; N, 12.23, found: C, 50.39; H, 4.25; N, 12.20.

2.5 Catalytic oxidation

2.5.1 The typical procedure for benzene oxidation. To an acetonitrile (3.0 mL) solution containing the catalyst (**1–3**) (2.5 μmol), TEA (5.0 μmol), and benzene (5.0 mmol) was added, similar to the procedure reported.[28] Then, aqueous hydrogen peroxide (2.5 mL, 25 mmol) was slowly added to the mixture using a syringe over 5 minutes under normal atmospheric conditions, and the reaction was stirred at 25/60 °C for 5 h. After 5 h, nitrobenzene was added to the reaction mixture as the internal standard and the catalyst was removed by passing it through a silica gel plug. Further, products were identified and quantified using GC/GC-MS. Calibration curves of authentic samples were used to calculate the benzene conversion and phenol yield. The catalytic oxidation was performed in triplicate, and the average value is reported.

2.5.2 Determination of kinetic isotope effect. To an acetonitrile (3 mL) solution of **1** (2.5 μmol), benzene (2.5 mmol), benzene-d_6 (2.5 mmol), and TEA (5.0 μmol) were added. Then, H_2O_2 (30%) (2.5 mL, 25 mmol) was added gradually under constant stirring, and the mixture was stirred at 60 °C for 5 h. After cooling it to room temperature, nitrobenzene was added as the internal standard. The catalyst was removed by passing the reaction mixture through a silica plug. Product analysis was done using GC/GC-MS, and the kinetic isotope effect (KIE) value for the reaction was determined by (moles of phenol)/(moles of phenol-d_5), similar to the procedure reported.[28]

2.5.3 Catalytic oxidation of aromatic substrates. To an acetonitrile (3.0 mL) solution containing catalyst **1** (2.5 μmol), the required aromatic substrate (5.0 mmol) and TEA (5.0 μmol) were added.[28] Then, aqueous H_2O_2 (2.5 mL, 25 mmol) was slowly added to the solution, and the reaction mixture was stirred at 60 °C for 5 h. After completion of the reaction, nitrobenzene was added as the internal standard (cyclohexanone was used as an internal standard in the case of nitrobenzene oxidation), and the products formed were identified and quantified using GC/GC-MS.

2.5.4 Benzene oxidation reaction with $H_2{}^{18}O$. The catalyst **1** (2.5 μmol) was dissolved in $H_2{}^{18}O$-acetonitrile mixture (v/v = 0.1 mL/1 mL). Then, TEA (2.5 μmol), benzene (0.5 mmol) and aqueous H_2O_2 (0.5 mL, 5 mmol) were added to the solution, and the reaction mixture was stirred at 60 °C for 5 h, similar to the procedure reported.[28] After adding the internal standard (nitrobenzene) and removing the catalyst, the products were analysed by GC-MS.

3 Results and discussion

3.1 Synthesis and characterisation of the ligands and nickel(II) complexes

The pentadentate monoamidate N5 ligands L1(H)–L3(H) were synthesised by adapting or modifying the known procedures, which involve the coupling of the corresponding secondary amines with 2-bromo-*N*-(quinoline-8-yl)acetamide (BrQ).[34] The nickel(II) complexes **1–3** were prepared by adding one equivalent of the monoanionic ligand (L1(H)–L3(H)) to a methanolic solution of $Ni(ClO_4)_2\cdot 6H_2O$, followed by the addition of one equivalent of triethylamine to complete ligand deprotonation. All the complexes are formulated as $[Ni(L)(H_2O)](ClO_4)$ based on ATR-IR, ^{1}H NMR, and UV-vis absorption spectroscopic techniques as well as HR-MS analysis. Moreover, the structural characterisation of a previously reported nickel(II) chloride complex ([Ni(L1)(Cl)]) containing ligand L1(H) revealed a distorted octahedral geometry around the nickel centre.[29] Similarly, the present complexes **1–3** are also expected to show octahedral geometry in the solution and solid state.

3.2 Electronic spectra

The electronic absorption spectra of complexes **1–3** were recorded in acetonitrile at room temperature (Fig. 1), and the data are summarised in Table 1. All the complexes exhibit two broad absorption bands in the range of 508–518 nm and 796–806 nm.

Besides, using the Tanabe–Sugano diagram, the peaks are assigned to the usually observed transitions of a nickel(II) ion having an octahedral environment. The high energy band in the range 508–518 nm is assigned to $^3A_{2g}(F) \rightarrow {}^3T_{1g}(F)$ (ν_2) transition, and the low energy broad band in the range 796–806 nm is assigned to $^3A_{2g}(F) \rightarrow {}^3T_{2g}(F)$ (ν_1). In addition, a weak shoulder

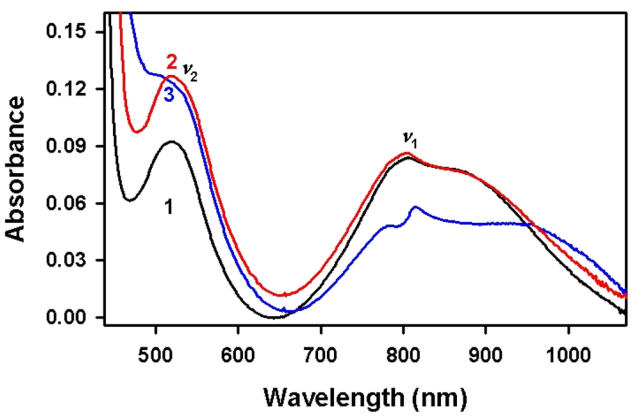

Fig. 1 UV-vis absorption spectra of the complexes **1–3** (4×10^{-3} M) in acetonitrile at room temperature.

Table 1 UV-Vis spectral data (λ_{max} in nm; ε in M^{-1} cm^{-1} in parentheses) of nickel(II) complexes **1–3** (4 mM) in acetonitrile at room temperature

	$^3A_{2g} \rightarrow {}^3T_{1g}(P)$ (ν_3)		$^3A_{2g} \rightarrow {}^3T_{1g}(F)$	$^3A_{2g} \rightarrow {}^3T_{2g}(F)$
Complex	Found	Calcd[a] (nm)	(ν_2), nm	(ν_1), nm
1	–	329	518 (23)	806 (21)
2	–	327	516 (41)	800 (21)
3	–	318	508 (31)	796 (12)

[a] Calculated by solving the quadratic equation and using B as 1080 cm^{-1}.

band was observed around 848–933 nm in all the complexes, which can be ascribed to the spin-forbidden transition $^3A_{2g}(F) \rightarrow {}^1E_{1g}(D)$. The band corresponding to $^3A_{2g}(F) \rightarrow {}^3T_{1g}(P)$ (ν_3) transition was not observed experimentally, presumably due to the overlap with the ligand-based high-energy transitions. However, using λ (nm) values of ν_1 and ν_2 transitions, ν_3 λ (nm) was calculated for all the complexes (**1**, 329 nm; **2**, 327 nm; **3**, 318 nm).[42]

These data are in good agreement with those of the previously reported octahedral nickel(II) complexes and confirm that complexes **1–3** possess octahedral geometry in solution.[27,36,38–41] In addition, the signals corresponding to ligands (0–12 ppm) disappeared in the ^1H NMR spectra of all the complexes, indicating the high-spin paramagnetic nature of these complexes (Fig. S15–S17). Also, the presence of a few paramagnetic ^1H NMR signals in the spectra confirmed the octahedral geometry of **1–3** in solution.[36]

3.3 Vibrational spectra

The infrared (IR) spectra of the ligands and complexes were recorded by employing the Attenuated Total Reflection (ATR) technique (see Fig. S1, S4, and S9). All the ligands exhibit the

Table 2 Optimisation of benzene oxidation reaction conditions using **1** with different catalyst loading, H_2O_2 concentration, temperature, and time

Entry	[1][a] (mol%)	Conversion (%)	Yield[e] (%)	Selectivity[f] (%)	TON[g]	TOF[h] (h^{-1})
1	0.025	16.3	16.2	99	648	129.6
2	0.050	25.1	24.6	98	492	98.4
3	0.075	26.3	25.2	96	336	67.2
4	0.100	27.8	25.6	92	256	51.2
5	0.125	30.0	25.9	86	207	41.4
6	0.150	31.2	26.1	84	174	34.8
Entry	$[H_2O_2]^b$ (mmol)	Conversion (%)	Yield (%)	Selectivity (%)	TON	TOF (h^{-1})
7	5	9.7	9.6	99	192	38.4
8	10	14.9	14.8	99	296	59.2
9	15	18.3	18.2	99	364	72.8
10	20	22.2	22.0	99	440	88.0
11	25	25.1	24.6	98	492	98.4
12	30	29.6	26.8	90	536	107.2
Entry	T[c] (°C)	Conversion (%)	Yield (%)	Selectivity (%)	TON	TOF (h^{-1})
13	25	12.9	12.8	99	256	51.2
14	40	16.5	16.3	99	326	65.2
15	60	25.1	24.6	98	492	98.4
16	80	27.2	24.9	91	498	99.6
17	100	29.0	24.5	84	490	98.0
Entry	Time[d] (h)	Conversion (%)	Yield (%)	Selectivity (%)	TON	TOF (h^{-1})
18	1	13.9	13.8	99	276	276.0
19	2	16.5	16.4	99	328	164.0
20	3	20.8	20.6	99	412	137.3
21	4	23.4	23.2	99	464	116.0
22	5	25.1	24.6	98	492	98.4
23	6	26.2	24.8	95	496	82.7
24	7	27.8	24.7	89	494	70.6
25	8	28.8	24.1	84	482	60.2

[a] Reaction conditions: benzene (5 mmol), TEA (5 μmol), H_2O_2 (25 mmol), 60 °C, 5 h. [b] Reaction conditions: benzene (5 mmol), TEA (5 μmol), **1** (2.5 μmol), 60 °C, 5 h. [c] Reaction conditions: benzene (5 mmol), TEA (5 μmol), **1** (2.5 μmol), H_2O_2 (25 mmol), 5 h. [d] Reaction conditions: benzene (5 mmol), TEA (5 μmol), **1** (2.5 μmol), H_2O_2 (25 mmol), 60 °C. [e] GC yield (reported values are the mean value of three determinations with a % error of 1). [f] Selectivity of phenol was calculated by [(phenol yield)/(yield of all products)] × 100. [g] Turnover number = concentration of phenol/concentration of catalyst. [h] Turnover frequency = Turnover number/time.

principal peaks in the range 3298–3315 cm^{-1} and 1671–1681 cm^{-1} corresponding to the N–H and C=O stretching frequencies, respectively. In all the complexes, the peak corresponding to N–H stretching disappeared, which indicated the deprotonation of amide nitrogen during the complex formation. In contrast, a broad peak around 3431–3484 cm^{-1} corresponding to O–H stretching from the coordinated aqua ligand was present. In addition, an intense peak in the range of 1091–1100 cm^{-1}, a sharp peak around 621–626 cm^{-1} and a weaker absorption peak at 976 cm^{-1} indicate the presence of uncoordinated ClO_4^- ions.[36,43] Collectively, the absence of N–H peak and the presence of O–H, C–N and uncoordinated ClO_4^- peaks in the ATR-IR spectra of all the complexes help to generally formulate the complexes as $[Ni(L)(H_2O)](ClO_4)$.

3.4 HR-MS analysis

HR-MS spectra of **1–3** were recorded in the positive ion mode in acetonitrile. All of them exhibited a molecular ion peak in the general form $[Ni(L)]^+$ at $m/z = 440.1020$ (for **1**, calcd = 440.1021) (Fig. S12), $m/z = 443.1124$ (for **2**, calcd = 443.1130) (Fig. S13), $m/z = 454.1192$ (for **3**, calcd = 454.1178) (Fig. S14). Also, all the complexes showed an additional peak corresponding to $[Ni(L(H))]^{2+}$ ion at $m/z = 220.5544$ (for **1**, calcd = 220.5550), $m/z = 222.0604$ (for **2**, calcd = 222.0605), $m/z = 227.5633$ (for **3**, calcd = 227.5628).

3.5 One-step selective oxidation of benzene to phenol

The catalytic activity of the synthesized nickel(II) complexes in the benzene oxidation reaction was investigated using aqueous H_2O_2 (30%) as the oxidant (Fig. S18), a method previously reported by us.[28] Catalytic conditions were optimised by screening the potential of complex **1** under various catalyst loadings, H_2O_2 concentration, temperature, and reaction time (Table 2 and Fig. S19) as phenol yield, selectivity, and TON were significantly affected by changes in these parameters. Even though maximum TON with 99% selectivity was achieved using 0.025 mol% catalyst, benzene conversion was only 16.3% (entry 1). Instead, 0.05 mol% catalysts resulted in better benzene conversion (24.6%) by maintaining the phenol selectivity as 98% (entry 2). However, a marginal improvement in the conversion (26.3%) and a drop-in selectivity (96%) were noted with further increment in the catalyst loading (entries 3–6). Similarly, the effect of oxidant amount was studied using H_2O_2 concentration in the 5–30 mmol range (entries 7–12). A gradual increase in the conversion was observed with an increase in the amount of H_2O_2 used. However, the optimum H_2O_2 concentration was found to be 25 mmol, as higher concentrations, such as 30 mmol, reduced the selectivity to 90% (entries 11 and 12). Although the reaction afforded 12.8% phenol at room temperature (25 °C), better conversions and TON were achieved at higher temperatures (entries 13–17). Nevertheless, the temperature above 60 °C favoured the formation of quinone and drastically reduced the phenol selectivity (entries 16 and 17). Similarly, reaction time also influenced the achieved conversion, selectivity, and TON of the catalysis (entries 18–25). A consistent rise in conversion was observed until 5 h, after which no significant increase in activity was noted. Also, the decrease in phenol selectivity at longer reaction times is attributed to quinone formation caused by over-oxidation. Further, the introduction of a base such as TEA to the reaction mixture improved the catalytic activity by facilitating the activation of H_2O_2. Therefore, a small quantity of TEA (5 μmol) was used for the reaction along with other reactants. Finally, under optimised reaction conditions (catalyst: 0.05 mol%, TEA: 5 μmol, benzene: 5 mmol, H_2O_2: 25 mmol in acetonitrile at 60 °C for 5 h), benzene oxidation was performed using all the catalysts (Table 3). Notably, complex **1** showed superior activity among the series with a phenol yield of 24.6%, a selectivity of 98% and a TON of 492. The electronic effect of the ligands on the catalytic performances of the complexes was visible as a decrease in the phenol yield (17.2%), and TON (344) was observed upon replacing one of the pyridyl arms in complex **1** with an imidazolyl methyl arm in complex **2**. Similarly, the introduction of a sterically constraining 6-methyl pyridyl group in complex **3** reduced the activity and afforded phenol with a yield of 7.0% and selectivity of 98%. The control experiments conducted in the absence of either the catalyst or TEA resulted in no formation of the phenol product. Notably, the present complexes exhibited superior catalytic activity than previously reported nickel complexes of sterically constraining ligands (Table S1). Also, the catalytic activity of complexes **1–3** in terms of phenol yield, selectivity, and TON was similar to that of known nickel catalysts with tripodal ligands (Table S1). Nevertheless, when compared to nickel complexes incorporating neutral N5 ligands, these anionic N5 ligand-based complexes demonstrated slightly diminished catalytic activity.[28]

Table 3 Catalytic benzene hydroxylation using complexes **1–3** under optimised reaction conditions[a]

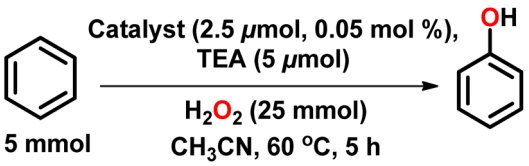

Catalyst	Temp. (°C)	Conversion (%)	Yield (%)	Selectivity (%)	TON	TOF (h^{-1})
1	25	12.9	12.8	99	256	51.2
	60	25.1	24.6	98	492	98.4
2	25	8.5	8.4	99	168	33.6
	60	17.5	17.2	98	344	68.8
3	25	—	—	—	—	—
	60	12	7	98	140	28

[a] Reaction conditions: benzene (5 mmol), TEA (5 μmol), catalyst (2.5 μmol), H_2O_2 (25 mmol), 60 °C, 5 h.

3.6 Oxidation of other aromatic substrates

The substrate scope of the reaction was extended to other aromatic compounds, such as toluene, ethylbenzene, cumene, chlorobenzene, nitrobenzene, and anisole, using catalyst **1**,

Table 4 Catalytic oxidation of other aromatic substrates using complex **1**

Entry	Substrate[a]	Yield[b] (%)	Selectivity
1	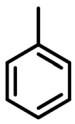	8	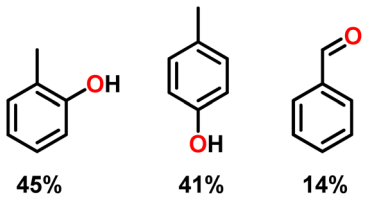 45% 41% 14%
2	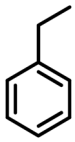	5	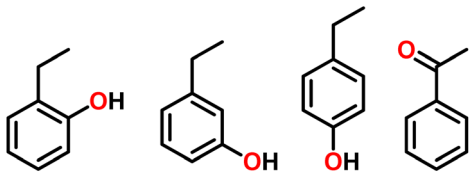 30% 21% 9% 40%
3	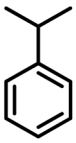	7	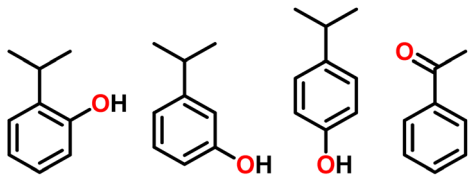 40% 25% 15% 20%
4	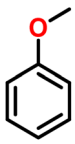	7	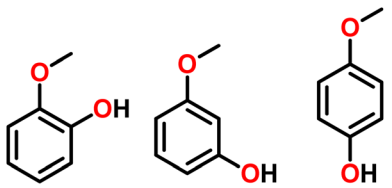 68% 26% 6%
5	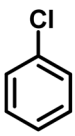	13	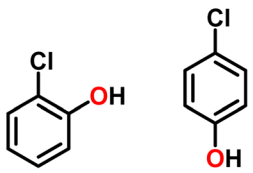 81% 19%
6	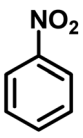	9	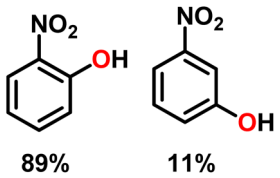 89% 11%

[a] Reaction condition: catalyst **1** (2.5 μmol), TEA (5.0 μmol), substrate (5.0 mmol) and H_2O_2 (2.5 mL, 25 mmol) in CH_3CN at 60 °C for 5 hours. [b] GC Yield.

adopting the optimised reaction conditions (Table 4).[28] The consistent selectivity for ring oxidation in all alkylated benzenes indicates that the catalysis proceeds through an electrophilic aromatic substitution mechanism (EAS). For instance, higher selectivity observed for *o*- and *p*-cresol (86% selectivity) in toluene oxidation can be correlated with the *ortho-para* directing of methyl groups in EAS. On the other hand, only a minor amount of benzaldehyde (14% selectivity) was obtained in this reaction due to side-chain oxidation (Scheme S1 and Fig. S20). Similarly, the oxidation of ethylbenzene majorly produced *-o*, *-m*, and *-p* ethylphenol (60% selectivity) along with acetophenone (40% selectivity) (Scheme S2 and Fig. S21). In cumene oxidation, a parallel trend was evident, producing *o*-, *m*-, and *p*-isopropyl phenol (80% selectivity) as the main products

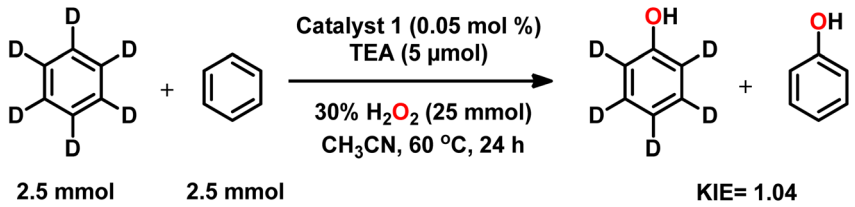

Scheme 2 Kinetic isotopic effect measurement using complex 1.

and benzaldehyde (20% selectivity) as a minor product (Scheme S3 and Fig. S22). The substrate anisole with an electron-releasing methoxy group favoured the formation of *o*- and *m*-methoxy phenol as the major products (94% selectivity) and *p*-methoxy phenol (6% selectivity) as the minor product (Scheme S4 and Fig. S23). In addition, *ortho-para* directing effect of chlorine was noted during the oxidation of chlorobenzene, where *o*- and *p*-chlorophenol (100% selectivity) were obtained without producing *meta* derivative (Scheme S5 and Fig. S24). Nitrobenzene, despite having an electron-withdrawing group, underwent oxidation to produce *o*- and *m*-nitrophenol (100% selectivity) (Scheme S6 and Fig. S25). Further, the use of phenol as the substrate did not afford any oxidised product (Fig. S26), revealing the selective mono-hydroxylation activity of the present complex. Overall, the preference for phenol production over alkane oxidation across all substrates implies that the oxidation reaction proceeds *via* an EAS mechanism.

3.7 Catalytic mechanism

Insights into the catalytic mechanism were obtained by performing a series of experiments. A KIE measurement was conducted using a 1 : 1 mixture of C_6D_6 and C_6H_6 with catalyst **1** (Scheme 2), and a KIE value of 1.04 was determined from the GC-MS/GC analysis of the phenol to phenol-d_5 ratio (Fig. S27) as similar to the previous reports.[23,24,28] Comparable inverse KIE values are reported for aromatic hydroxylation reactions catalysed by various first–row transition metal complexes, proceeding *via* EAS with metal-bound oxygen species as reactive intermediates.[24,44–48] In addition, such a small KIE value rules out the possibility of a hydroxyl radical (Fenton-type) mechanism (KIE: 1.7) or metal insertion reaction (KIE: 2.9–4.8) in the catalytic cycle.[49–51] In the case of previously employed nickel(II) complexes, a KIE value of ~1 is obtained, and the presence of dinickel(III) bis(μ-oxo) species was suggested in their catalytic cycle. However, recent DFT studies support the role of a nickel-oxyl species as the key reactive species in benzene oxidation mediated by nickel complexes.[26,28]

In addition, the reaction carried out using $H_2{}^{18}O$ and H_2O_2 displayed almost no ^{18}O atom incorporation into the produced phenol (Fig. S28). Further, the oxidation of *cis*-1,2-dimethylcyclohexane afforded cis hydroxylated (6%) as the major product and a trace amount of trans product (<1%) (Fig. S29). Stereo retention observed in this reaction also helped us to rule out the Fenton-type mechanism. Additionally, the oxidation

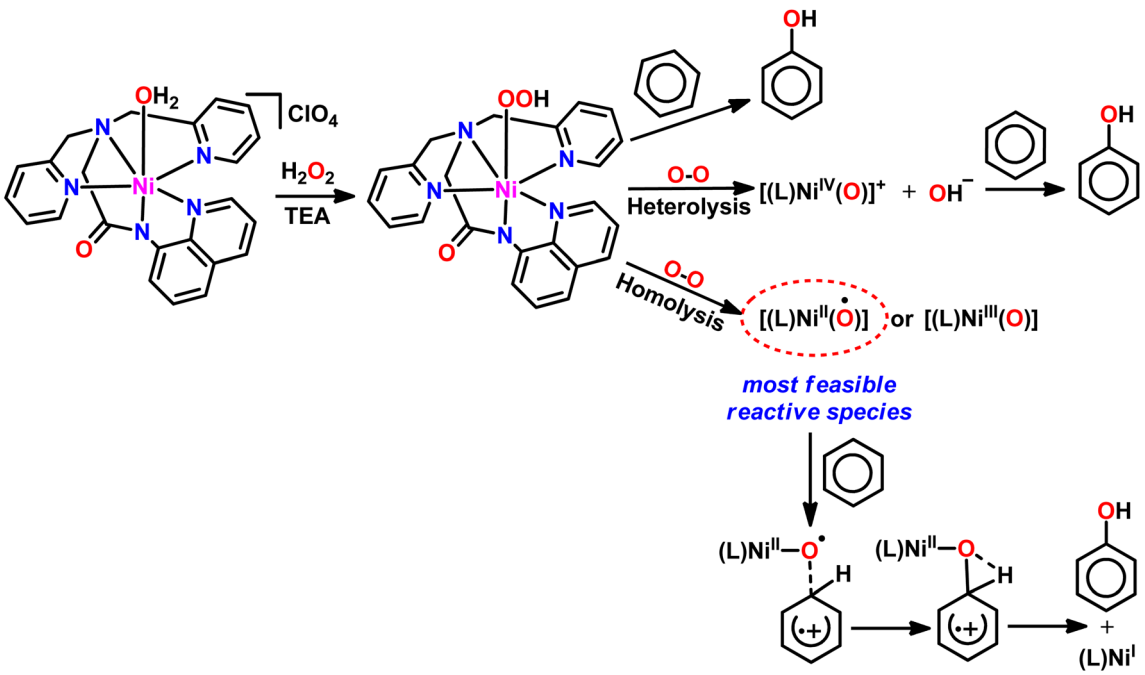

Fig. 2 The plausible mechanism for the oxidation of benzene catalysed by 1.

reaction was performed in the presence of radical trapping agents such as CCl_4 and TEMPO (2,2,6,6-tetramethyl piperidine-1-yl-oxyl) to monitor the quenching of catalytic activity. However, the phenol yield remained unaffected by the presence or absence of CCl_4/TEMPO, indicating that carbon-centred radicals are not involved in the reaction (Fig. S30 and S31). Similarly, cyclohexane oxidation in the presence of CCl_4 produced cyclohexanol and cyclohexanone (95% combined selectivity) and cyclohexyl chloride (5%) (Fig. S32). These results exclude the Fenton-type and carbon-centre radical type reaction under our experimental conditions.

In the present study, the formation of a dinickel(III) bis(μ-oxo) species similar to precedent nickel(II) complexes of N4 ligands is unlikely to happen because of the unavailability of a second labile site for the coordination of a bridging oxygen atom. Despite that, the breakage of one of the Ni–N bonds to provide an additional vacant site for the coordination of bridging oxygen atoms to form a dinickel(III) bis(μ-oxo) complex cannot be completely ruled out. The most possible mechanism would be the generation of a [(L)Ni^{II}(OOH)] intermediate and the subsequent O–O homolysis or heterolysis to form [(L)Ni^{III}(O)]/[(L)Ni^{II}($O^{\bullet}$)] or [(L)Ni^{IV}(O)]$^+$ (Fig. 2). The formation of such nickel oxygen species is reported for hydroxylation of alkanes and benzene catalysed by nickel(II) complexes of a series of N5 ligands and epoxidation catalysed by nickel(II) chloride complex of L1(H) ([Ni(L1)(Cl)]).[27–30] Moreover, our recent experimental mechanistic investigation on aromatic oxidation using nickel(II) complexes of neutral pentadentate N5 ligands gave comparable results.[28] Also, the related theoretical studies implicate the thermodynamic feasibility for the formation of [(L)Ni^{II}($O^{\bullet}$)] and its subsequent reactivity with benzene to produce phenol.[28] Therefore, the catalytic cycle driven by [(L)Ni^{II}($O^{\bullet}$)] species is expected in the present study as well. However, further studies are required to understand the clear mechanistic picture of benzene hydroxylation catalysed by complexes **1–3**.

4 Conclusion

Three nickel(II) complexes (**1–3**) of monoamidate pentadentate ligands were synthesised, characterised, and employed as catalysts in a one-step benzene hydroxylation reaction with H_2O_2 as the oxidant. Complex **1** showed superior activity among the series with a phenol yield of 24.6%, selectivity of 98%, and a turnover number of 492 under optimal reaction conditions. Replacement of one of the pyridyl moieties in catalyst **1** with imidazolyl methyl (**2**) or 6-methyl pyridyl 1-methyl (**3**) groups decreased the catalytic activity in terms of benzene conversion by maintaining the phenol selectivity. Further, the inverse kinetic isotopic effect (1.04) obtained for the reaction rules out the Fenton-type reaction pathway and suggests the involvement of the EAS mechanism mediated by a nickel-oxygen species. Moreover, preferential ring oxidation over side-chain oxidation and *o*/*m*/*p*-product distribution pattern obtained for other aromatic substrates support the EAS mechanism. Nevertheless, further studies are required to identify the key reactive species responsible for the oxidation reaction.

Conflicts of interest

There are no known conflicts of interest to declare.

Note added after first publication

This article replaces the version published on 5th November 2025, which included incorrect details for ref. 18.

Data availability

The data supporting this article have been included as part of the supplementary information (SI). Supplementary information: we provide all the relevant characterisation data, chromatograms (Fig. S1–S33), a comparison with the existing data (Table S1), and a summary of the mechanistic study. See DOI: **https://doi.org/10.1039/d5ra07204b**.

Acknowledgements

M. S. acknowledges the Science and Engineering Research Board (SERB) for the CRG grant (CRG/2023/002850) and the National Institute of Technology Calicut for the Faculty Research Grant. A. R. sincerely thank the UGC-SRF for providing her with the fellowship to support her PhD studies. S. M. acknowledges the Spanish Ministry of Science (FJC2021-047874-I) for providing the fellowship to support his research work. We thank the CMC, NIT Calicut, for NMR characterisation. Also, we thank the Department of Chemistry, NIT Calicut, for providing the HRMS facility. We thank Prof. Miquel Costas, IQCC, Universitat de Girona, Spain, for helping us to record GC/GC-MS.

References

1 M. Weber, M. Weber, M. Kleine-Boymann, in *Ullmann's Encyclopedia of Industrial Chemistry*, Wiley, 2020, pp. 1–20.
2 H. Hock, S. Lang and B. Dtsch, *Chem. Ges. B*, 1944, **77**, 257–264.
3 A. Rajeev, M. Balamurugan and M. Sankaralingam, *ACS Catal.*, 2022, **12**, 9953–9982.
4 M. Sono, M. P. Roach, E. D. Coulter and J. H. Dawson, *Chem. Rev.*, 1996, **96**, 2841–2888.
5 E. I. Solomon, A. Decker and N. Lehnert, *Proc. Natl. Acad. Sci. U.S.A.*, 2003, **100**, 3589–3594.
6 G. M. Whited and D. T. Gibsont, *J. Bacteriol.*, 1991, **173**, 3010–3016.
7 M. Costas, M. P. Mehn, M. P. Jensen and L. Que, *Chem. Rev.*, 2004, **104**, 939–986.
8 L. Que and W. B. Tolman, *Nature*, 2008, **455**, 333–340.
9 D. Mansuy, *CR Chim.*, 2007, **10**, 392–413.
10 G. Mukherjee, J. K. Satpathy, U. K. Bagha, M. Q. E. Mubarak, C. V. Sastri and S. P. De Visser, *ACS Catal.*, 2021, **11**, 9761–9797.
11 W. Nam, *Acc. Chem. Res.*, 2007, **40**, 522–531.
12 T. Punniyamurthy, S. Velusamy and J. Iqbal, *Chem. Rev.*, 2005, **105**, 2329–2363.

13 T. P. Mohammed, A. George, M. P. Sivaramakrishnan, P. Vadivelu, S. Balasubramanian and M. Sankaralingam, *J. Inorg. Biochem.*, 2023, **247**, 112309.
14 A. S. Thennarasu, T. P. Mohammed and M. Sankaralingam, *New J. Chem.*, 2022, **46**, 21684–21694.
15 R. Mayilmurugan, M. Sankaralingam, E. Suresh and M. Palaniandavar, *Dalton Trans.*, 2010, **39**, 9611–9625.
16 T. P. Mohammed, M. Velusamy and M. Sankaralingam, *J. Inorg. Biochem.*, 2025, **270**, 112906.
17 T. P. Mohammed, S. Roy and M. Sankaralingam, *Inorg. Chim. Acta*, 2025, **574**, 122372.
18 T. P. Mohammed, K. G. Sharma, M. P. Sivaramakrishnan, S. Muthuramalingam, P. Vadivelu, M. Velusamy and M. Sankaralingam, *J. Inorg. Biochem.*, 2026, **275**, 113120.
19 A. Rajeev, T. P. Mohammed, A. George and M. Sankaralingam, *Chem. Rec.*, 2025, **25**, e202400186.
20 A. C. Lindhorst, S. Haslinger and F. E. Kühn, *Chem. Commun.*, 2015, **51**, 17193–17212.
21 R. V. Ottenbacher, E. P. Talsi and K. P. Bryliakov, *Appl. Organomet. Chem.*, 2020, **34**, 1–25.
22 S. Fukuzumi and K. Ohkubo, *Asian J. Org. Chem.*, 2015, **4**, 836–845.
23 Y. Morimoto, S. Bunno, N. Fujieda, H. Sugimoto and S. Itoh, *J. Am. Chem. Soc.*, 2015, **137**, 5867–5870.
24 S. Muthuramalingam, K. Anandababu, M. Velusamy and R. Mayilmurugan, *Catal. Sci. Technol.*, 2019, **9**, 5991–6001.
25 E. Masferrer-Rius, R. M. Hopman, J. van der Kleij, M. Lutz and R. J. M. K. Gebbink, *Chimia*, 2020, **74**, 489–494.
26 K. Farshadfar and K. Laasonen, *Inorg. Chem.*, 2024, **63**, 5509–5519.
27 M. Sankaralingam, M. Balamurugan, M. Palaniandavar, P. Vadivelu and C. H. Suresh, *Chem. Eur. J.*, 2014, **20**, 11346–11361.
28 A. Rajeev, S. Muthuramalingam, V. P. Murugan, M. Costas, P. Vadivelu and M. Sankaralingam, *ChemCatChem*, 2025, **17**, e202401645.
29 K. H. Bok, M. M. Lee, G. R. You, H. M. Ahn, K. Y. Ryu, S. J. Kim, Y. Kim and C. Kim, *Chem. Eur. J.*, 2017, **23**, 3117–3125.
30 M. Sankaralingam, M. Balamurugan and M. Palaniandavar, *Coord. Chem. Rev.*, 2020, **403**, 213085.
31 M. Sankaralingam, Y. M. Lee, D. G. Karmalkar, W. Nam and S. Fukuzumi, *J. Am. Chem. Soc.*, 2018, **140**, 12695–12699.
32 D. G. Karmalkar, M. Sankaralingam, M. S. Seo, R. Ezhov, Y. M. Lee, Y. N. Pushkar, W. S. Kim, S. Fukuzumi and W. Nam, *Angew. Chem., Int. Ed.*, 2019, **58**, 16124–16129.
33 M. Sankaralingam, Y. M. Lee, Y. Pineda-Galvan, D. G. Karmalkar, M. S. Seo, S. H. Jeon, Y. Pushkar, S. Fukuzumi and W. Nam, *J. Am. Chem. Soc.*, 2019, **141**, 1324–1336.
34 Y. Hitomi, K. Arakawa, T. Funabiki and M. Kodera, *Angew. Chem., Int. Ed.*, 2012, **51**, 3448–3452.
35 Y. Hitomi, K. Arakawa and M. Kodera, *Chem. Eur. J.*, 2013, **19**, 14697–14701.
36 (*a*) A. Das, A. Rajeev, S. Bhunia, M. Arunkumar, N. Chari and M. Sankaralingam, *Inorg. Chim. Acta*, 2021, **526**, 120515; (*b*) M. Molla, A. Saha, S. K. Barman and S. Mandal, *Chem. Eur. J.*, 2024, **30**, e202401163.
37 A. Rajeev, A. T. Thomas, A. Das and M. Sankaralingam, *Eur. J. Inorg. Chem.*, 2024, **27**, e202400205.
38 S. Patra, A. Das, S. Bhunia, A. Rajeev and M. Sankaralingam, *Catal. Today*, 2023, **423**, 113972.
39 A. Rajeev, S. Muthuramalingam and M. Sankaralingam, *RSC Adv.*, 2024, **14**, 30440–30451.
40 M. Sankaralingam, P. Vadivelu, E. Suresh and M. Palaniandavar, *Inorg. Chim. Acta*, 2013, **407**, 98–107.
41 M. Sankaralingam, P. Vadivelu and M. Palaniandavar, *Dalton Trans.*, 2017, **46**, 7181–7193.
42 A. B. P. Lever, *J. Chem. Edu.*, 1968, **45**, 711–712.
43 E. Wickenden, A. Krause and I. Nickel, *Inorg. Chem.*, 1964, **4**, 404–407.
44 S. Muthuramalingam, K. Anandababu, M. Velusamy and R. Mayilmurugan, *Inorg. Chem.*, 2020, **59**, 5918–5928.
45 K. Anandababu, S. Muthuramalingam, M. Velusamy and R. Mayilmurugan, *Catal. Sci. Technol.*, 2020, **10**, 2540–2548.
46 A. Raba, M. Cokoja, W. A. Herrmann and F. E. Kühn, *Chem. Commun.*, 2014, **50**, 11454–11457.
47 G. Capocasa, G. Olivo, A. Barbieri, O. Lanzalunga and S. Di Stefano, *Catal. Sci. Technol.*, 2017, **7**, 5677–5686.
48 E. Masferrer-Rius, M. Borrell, M. Lutz, M. Costas and R. J. M. K. Gebbink, *Adv. Synth. Catal.*, 2021, **363**, 3783–3795.
49 R. Augusti, A. O. Dias, L. L. Rocha and R. M. Lago, *J. Phys. Chem. A*, 1998, **102**, 10723–10727.
50 M. H. Emmert, A. K. Cook, Y. J. Xie and M. S. Sanford, *Angew. Chem., Int. Ed.*, 2011, **50**, 9409–9412.
51 A. Rajeev, M. Sankaralingam, in *Oxygen Atom Transfer Reactions*, Bentham Science, Singapore, 2023, pp. 62–90.